Phosphorescence excitation mapping and vibrational spectroscopy of HC9N and HC11N cyanopolyynes in organic solvents

Urszula Szczepaniak, Kazunori Ozaki, Kaito Tanaka, Yuma Ohnishi, Yoriko Wada, Jean-Claude Guillemin, Claudine Crépin, Robert Kolos, Yusuke Morisawa, Hal Suzuki, et al.

Credit Author Statement:

Ms. Ref. No.: MOLSTRUC-D-20-00568

Dr. Urszula Szczepaniak: As the leading researcher of this project, she presented initial idea of phosphorescence experiments and started the collaboration by visiting Kindai University.

Mr. Kazunori Ozaki: In the early stage of the phosphorescence experiments in Kindai University, he supported the sample preparation with various polyyne moleules.

Mr. Kaito Tanaka: He worked for preparation of purified solution samples of cyanopolyyne molecules for detailed phosphorescence spectroscopy.

Mr. Yuma Ohnishi: For the IR absorption spectroscopy, he prepared preparative-scale sample solutions of HC_9N and $HC_{11}N$.

Dr. Yoriko Wada: Serving as the instructor on sample preparation, she measured IR absorption spectra of HC_9N and $HC_{11}N$ with careful treatments of sample concentration and volumes.

Prof. Jean-Claude Guillemin: As an expert of the cyanopolyyne research, he gave the ideas for treatments of the reactive cyanopolyyne molecules.

Prof. Claudine Crépin: As a pioneer of the phosphorescence spectroscopy of matrix isolated cyanopolyyne molecules, comments and discussions are given to the present spectroscopic data.

Prof. Robert Kołos: As an expert of the spectroscopy of matrix isolated cyanopolyynes, discussions are made for the interpretation of spectra, especially phosophorescence.

Prof. Yusuke Morisawa: His expertise on vibrational spectroscopy was highly appreciated upon the discussion of the IR and Raman spectra of cyanopolyyne molecules.

Dr. Hal Suzuki: He worked for the development of the experimental setup of the cryogenic system for phosphorescence spectroscopy.

Prof. Tomonari Wakabayashi: Phosphorescence spectroscopy and interpretation of the spectra were conducted under his leadership.

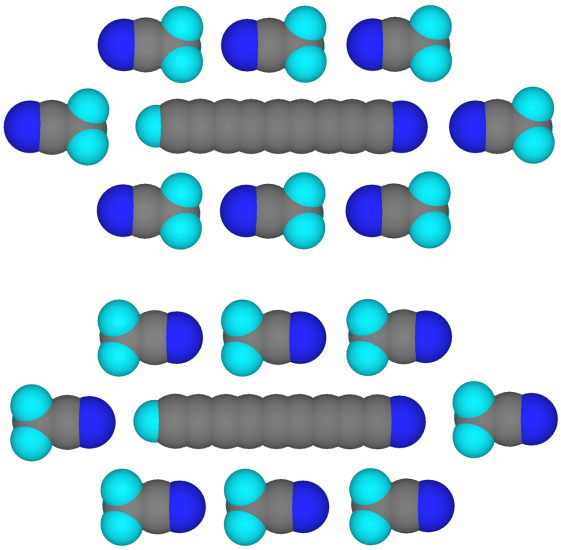

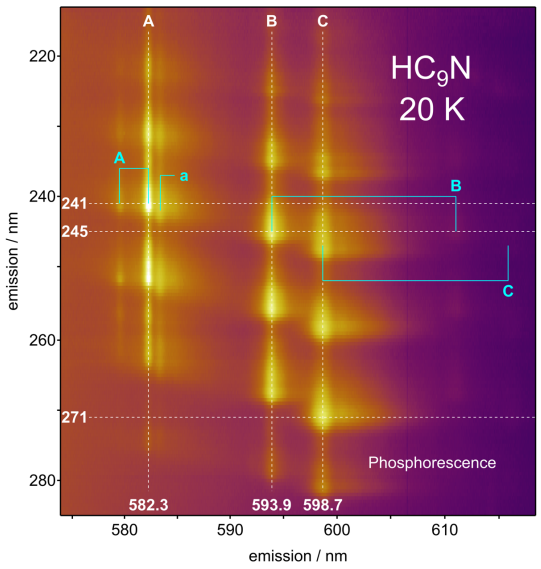
A
B
C
HC9N
20 K
A
a
B
C
241
245
271
Phosphorescence
582.3
593.9
598.7
220
240
260
280
580
590
600
610
emission / nm
emission / nm

Resubmitted on 2020.4.1 after revision.
J. Mol. Struct, Special Issue dedicated to Prof. Zofia Mielke.

Phosphorescence excitation mapping and vibrational spectroscopy of HC_9N and $HC_{11}N$ cyanopolyynes in organic solvents

Urszula Szczepaniak,[1] Kazunori Ozaki,[2] Kaito Tanaka,[2] Yuma Ohnishi,[2] Yoriko Wada,[2] Jean-Claude Guillemin,[3] Claudine Crépin,[4] Robert Kołos,[5] Yusuke Morisawa,[2] Hal Suzuki,[2] and Tomonari Wakabayashi[2*]

[1] *IRsweep, Laubisrütistrasse 44, 8712 Stäfa, Switzerland*
[2] *Department of Chemistry, Kindai University, Higashi-Osaka 577-8502, Japan*
[3] *Univ Rennes, Ecole Nationale Supérieure de Chimie de Rennes, CNRS, ISCR - UMR 6226, F-35000 Rennes, France*
[4] *Université Paris-Saclay, CNRS, Institut des Sciences Moléculaires d'Orsay, 91405, Orsay, France*
[5] *Institute of Physical Chemistry, Polish Academy of Sciences, Kasprazaka 44/52, Warsaw 01-224, Poland*

[*]Email: wakaba@chem.kindai.ac.jp

Abstract

Cyanopolyyne molecules, HC_9N and $HC_{11}N$, were isolated in solutions and UV, IR, and resonance Raman spectra were measured for the study of their electronic and vibrational properties. Strong signals were observed both in the IR and resonance Raman spectra for the stretching vibrational mode of the sp-hybridized linear carbon chain in the electronic ground state, *i.e.*, σ_4 at 2141 cm^{-1} for HC_9N and σ_6 at 2105 cm^{-1} for $HC_{11}N$. Trapped in cryogenic solid acetonitrile matrix hosts at 20 K, transitions in phosphorescence, $\tilde{a}^3\Sigma^+ \rightarrow \tilde{X}^1\Sigma^+$, were observed for HC_9N at 582.3 nm (0-0) and longer wavelengths and for $HC_{11}N$ at 643.7 nm (0-0) and longer wavelengths. Electronic transitions in the UV, $^1\Sigma^+ \leftarrow \tilde{X}^1\Sigma^+$, were elucidated by phosphorescence excitation mapping to observe asymmetric patterns with sharp emission-absorption features explainable by Shpolsky effects. For HC_9N, three distinct trapping sites were discernible in solid acetonitrile, while the phosphorescence spectra were blurred in solid *n*-hexane. The observed phosphorescence lifetime of HC_9N was longer than that of

$HC_{11}N$, comparable to the trend reported for the series of cyanopolyyne molecules in solid krypton matrix hosts.

Introduction

Cyanopolyynes, a series of sp-hybridized linear carbon chain molecules terminated by a hydrogen atom at one end and by a cyano-group at the other, $H(C{\equiv}C)_nC{\equiv}N$, have been targets of spectroscopic investigations both in space and laboratories [1-12]. Rotationally resolved spectra of microwave emission are widely used for the detection of the series of molecules and are exploited as a probe for molecular evolutions in circumstellar shells of red giants or late AGB stars as well as in molecular clouds [1-5]. Synthetic cyanopolyynes are accessible in the laboratory for gas phase spectroscopy and matrix isolation spectroscopy [6-11]. Photochemistry undergoes in inert cryogenic matrices and is explored to elongate the carbon chain of cyanopolyyne molecules [7-9]. Recently, phosphorescence of cyanopolyynes, HC_5N, HC_7N and HC_9N, was detected in solid rare-gas matrices at cryogenic temperature and their vibronic spectra were obtained as action spectra by phosphorescence excitation [9,10,12]. Methylcyanopolyynes are also target molecules for spectroscopy [13-15]. Laser ablation of carbon particles in liquid acetonitrile has opened a way for production of longer polyynes and cyanopolyynes in a milligram order to handle them in organic solvents under ambient temperature [16-20]. Further stabilization is acquired for hydrogen-capped polyyne molecules trapped in solid host environments such as single wall carbon nanotubes (SWNTs) [21-23] and polyvinyl alcohol (PVA) [24].

Increasing interests on carbon species of sp-hybridization are found in the field of nanomaterials as well as astrochemistry. The series of cyanopolyyne molecules, now accessible in the laboratory, are promising model compounds not only for spectroscopy but also for building blocks of novel compounds of sp-hybridized linear carbon chain species. As the interstellar molecules, the presence of HC_9N has been confirmed based on microwave emission spectroscopy of molecular rotational transitions [1,3,4], while the detection of $HC_{11}N$ was negated recently by estimating its abundance below an expected amount from the extrapolation [5]. When they are detected in other spectral regions by their electronic and vibrational transitions, the spectral information not only

reconfirms their abundance in space, especially $HC_{11}N$, but also provides data for the study of photochemical conditions in the interstellar medium.

Matrix isolation spectroscopy combined with theoretical interpretation based on *ab initio* molecular orbital calculations has been extensively developed as a powerful tool for thorough studies of photochemistry, molecular structures, and intermolecular interactions of reactive species at cryogenic temperature [25-27]. We report here spectroscopic investigations of two cyanopolyynes, namely HC_9N and $HC_{11}N$ in solutions at ambient temperature, by UV absorption, infrared (IR) absorption, and resonance Raman spectroscopy. Phosphorescence spectra of HC_9N and $HC_{11}N$ are measured in cryogenic matrix hosts of solid acetonitrile or *n*-hexane at 20 K. Phosphorescence excitation mapping is performed for comparison with UV absorption spectra in the solutions to discuss the presence of multiple trapping sites and host-guest interactions in the solid matrices.

Experimental

Sample preparation and UV absorption spectroscopy

Preparation and characterization of laser ablated polyyne molecules are described elsewhere [16-20]. Briefly, cyanopolyyne molecules are formed by laser ablation (Continuum Powerlite 8010, 1064 nm, 0.5 J/pulse, 10 Hz) of graphite particles suspended in acetonitrile (Nacalai Guaranteed Reagent, Acetonitrile, ≥99.5 % CH_3CN) and separated in size by high performance liquid chromatography (HPLC) [17]. UV absorption spectra are measured for checking purity and for adjusting concentration by using a spectrophotometer (Jasco V-670). Similarly to the hydrogen-capped polyynes [28], cyanopolyynes have molar absorption coefficients of ~10^5 L mol^{-1} cm^{-1}. Disregarding vibronic details, interpolated UV absorption coefficients of $\varepsilon \approx 2.2\times10^5$ and $\approx 2.7\times10^5$ L mol^{-1} cm^{-1} are applicable to HC_9N and $HC_{11}N$, respectively. For spectroscopy in *n*-hexane, cyanopolyyne molecules, *e.g.*, HC_9N, are extracted from the solution of acetonitrile into *n*-hexane, then residual acetonitrile is removed by HPLC eluted by *n*-hexane (Kishida Chameleon Reagent, Hexane, >96% *n*-hexane).

IR absorption spectroscopy

For IR absorption spectroscopy [20], a few milligrams of HC_9N molecules are extracted into *n*-hexane, concentrated by evaporating *n*-hexane to a volume of ≈3 mL, and ≈3 mL of carbon tetrachloride, CCl_4, is added then evaporated further to a volume of ≈3 mL. Residual *n*-hexane is removed from the crude CCl_4 solution of HC_9N using HPLC eluted by CCl_4 and the resulting fraction of HC_9N/CCl_4 is concentrated by evaporation to a volume of ≈0.5 mL for the IR measurement.

The 0.1-mm-pathlength IR cell with KBr windows is filled with the solution of HC_9N or $HC_{11}N$ in CCl_4 at a concentration of ~10^{-2} mol L^{-1}. IR absorption spectra are measured at ambient temperature in a range of 400 - 4000 cm^{-1} at a resolution of 1.0 cm^{-1} using an FTIR spectrometer (Nicolet Magna 750, KBr beam splitter, DTGS detector) [20]. Whole system is covered by a rubber-sealed container box and purged inside with dry nitrogen (Iwatani N_2-gas generator GN-20, 20 L/min) to diminish absorption lines of water vapor and carbon dioxide.

Resonance Raman spectroscopy

Concentration of HC_9N in liquid *n*-hexane is adjusted to the absorbance of A = 0.6 - 1.2 at the UV absorption maximum for the optical pathlength of 1.0 cm. A transparent 1.0-cm quartz cell filled with the 4-mL solution in *n*-hexane is placed in a cell holder where the solution is photoexcited by a pulsed UV laser beam of a 4-mm diameter (Sirah Cobra Dye/SHG or VersaScan MB/uvScan OPO/SHG, pumped by 3rd harmonics of INDI-40 Nd:YAG) [18]. The excitation wavelength was tuned at 264 nm (Coumarin 153/SHG) for HC_9N and at 274 nm (OPO/SHG) for $HC_{11}N$. The scattered light perpendicular to both directions of propagation and polarization of the linearly polarized laser beam was collected by a quartz lens and routed to the entrance slit of the UV spectrometer (McPherson Model 209, f = 1.33 m, 1200 G/mm blazed at 300 nm) equipped with an array detector (PI ICCD 1024×256 pixels, ST138). The resonance

Raman scattering spectra are transferred to a PC using WinSpec 3.2 and processed by Igor Pro 8.04.

Phosphorescence Spectroscopy

The purified solution of HC_9N or $HC_{11}N$ is concentrated to a volume of ≈1.0 mL to have a concentration of ~10^{-3} mol L^{-1} and introduced through a 1/16-inch tubing into a vacuum system at ~10^{-5} Pa of the cryostat (Daikin V202CL). The solution is sprayed then condensed onto the surface of a copper slab cooled at 20 K in the cryostat to form millimeters-thick solid matrix samples of the mixture, HC_9N/CH_3CN, HC_9N/*n*-hexane, or $HC_{11}N/CH_3CN$. Phosphorescence signals are recorded by three measurement modes: (1) dispersed phosphorescence spectra are recorded at a fixed excitation wavelength using a spectrometer (PI320, f = 0.3 m, 1200 G/mm blazed at 500 nm or 600 G/mm blazed at 1000 nm) equipped with a liquid-N_2-cooled array detector (PI PyLoN, OE256), (2) dispersed phosphorescence spectra are recorded redundantly during the excitation-wavelength scan in a range of 213 - 302 nm with an increment of 0.5 nm using a spectrometer (Acton SP300i, f = 0.3 m, 1200 G/mm blazed at 500 nm or 600 G/mm blazed at 500 nm) equipped with an array detector (PI SPEC10), and (3) phosphorescence excitation spectra are recorded on a digitizing oscilloscope (LeCroy WavePro 954) by plotting the phosphorescence intensity at a fixed wavelength during the excitation-wavelength scan using a photomultiplier detector (Hamamatsu R928). For the mode (3), a time window, *e.g.*, between 2 and 20 msec, is set to avoid instantaneous scattering upon the excitation pulse for collecting only delayed emission to smooth out the relatively featureless background. To suppress the second-order dispersion of the grating spectrometers, colored glass filters (Schott long-pass filters, GG395, GG475, or OG570) are used for cutting the shorter wavelength light. Phosphorescence mapping is made from the series of spectra in the mode (2), while phosphorescence lifetimes are obtained from the decay profile in the mode (3). Commonly for the three modes (1) - (3), excitation is performed by using a tunable pulsed laser system (GWU VersaScan MB/uvScan OPO/SHG pumped by 3rd

harmonics of INDI-40 Nd:YAG, 7 nm duration) and the wavelength is calibrated and monitored by using a wavelength meter (GWU LambdaScan).

Results and discussion

A. UV, IR, and Raman spectra in solutions

Figure 1 shows UV absorption spectra of HC_9N and $HC_{11}N$ in *n*-hexane. The absorption maximum is at 245.6 nm for the former and at 264.4 nm for the latter. In addition to the vibrational progression of a stretching mode toward shorter wavelengths, which is similar to the spectra of hydrogen-capped polyynes, $H(C{\equiv}C)_nH$ [16,18-20,28], shoulders and weaker bands are discernible in the longer wavelength region [17]. Transitions to electronic excited states, to which the transition from the ground state is symmetry forbidden for centrosymmetric $H(C{\equiv}C)_nH$ molecules of $D_{\infty h}$ symmetry, are activated for asymmetric $H(C{\equiv}C)_nC{\equiv}N$ molecules of $C_{\infty v}$ symmetry and observed as a part of the allowed transition, $^1\Sigma^+ \leftarrow \tilde{X}^1\Sigma^+$. The observed UV absorption features are summarized in Table 1.

Figure 1.

Table 1.

Figure 2 shows IR and resonance Raman spectra for HC_9N and $HC_{11}N$. Stretching modes of the sp-carbon chain are peaking in a range of 2028 - 2239 cm^{-1} for both molecules. Among others, the strongest peaks at 2141 cm^{-1} for HC_9N and at 2105 cm^{-1} for $HC_{11}N$ are downshifting with the increasing carbon chain length, while the frequencies of the modes at high and low frequency ends do not depend on the carbon chain length (for vibrational properties by B3LYP/cc-pVQZ molecular orbital calculations, see Table S1 and Figs. S1 and S2 in supplementary data). All the stretching σ modes in this frequency region of 2150 ± 150 cm^{-1}, namely 5 modes, σ_2 - σ_6, for HC_9N and 6 modes, σ_2 - σ_7, for $HC_{11}N$, are both IR and Raman active for cyanopolyynes of $C_{\infty v}$ symmetry, though some of them have only negligible intensities, *e.g.*, the IR σ_4 mode of $HC_{11}N$. The highest frequency peak in this region, *i.e.*, σ_2 at

2239 cm^{-1} for HC_9N and σ_2 at 2235 cm^{-1} for $HC_{11}N$, appears with substantial IR absorption intensity relative to the main peak, while the corresponding Raman mode signal is relatively weak. In this collective stretching mode of the $–(C≡C)_n–C≡N$ chain, the bond length of the polarized C≡N bonding changes relatively largely compared to the other stretching modes at lower frequencies. Conversely, the lack of these bands in the measured Raman spectra is coherent with their expected weakness (for calculated intensities, see Table S1 and Ref. 12). For both HC_9N and $HC_{11}N$, strong IR signals were observed for the highest frequency CH stretching σ_1 mode at 3302 - 3303 cm^{-1} and for the low frequency CH bending π mode at 626 - 532 cm^{-1} (not shown in Fig. 2). The observed IR and Raman peaks are compiled in Table 2.

Figure 2.

Table 2.

For HC_9N, a weak IR absorption at 2174 cm^{-1} is an order of magnitude stronger for the predicted intensity for σ_3 and assigned to an overtone of the pseudosymmetric σ_8 stretching mode [12]. For $HC_{11}N$, a group of IR absorption lines including the strongest signal at 2105 cm^{-1} and those in its vicinity are attributable to σ_6, which is strongly perturbed by overtones and/or combinations. The nearby σ_5 mode is possibly perturbed also.

Note here that, for the resonance Raman spectroscopy, the excitation wavelength was tuned to a maximum or an edge of a weaker UV absorption band at longer wavelength to avoid serious self-absorption of Stokes lines. During the measurement of the Raman spectra, decay of the Raman signals was observed for the target molecule and some additional signals appear, *e.g.*, a peak with an asterisk in the Raman spectrum of HC_9N in Fig. 2, indicating decomposition of HC_9N molecules in *n*-hexane upon absorption of the UV photons for the excitation.

B. Phosphorescence of HC_9N

Figure 3 plots dispersed phosphorescence spectra of HC_9N molecules trapped in solid acetonitrile at 20 K. Typical spectra are shown in Fig. 3a for which the excitation wavelength is set at 250.0, 255.0, or 271.0 nm. Four bands in the electronic transition, $\tilde{a}^3\Sigma^+ \rightarrow \tilde{X}^1\Sigma^+$, are observed upon the 250.0-nm excitation with maxima at 582.3, 665.4, 775.6, and 927.8 nm for 0-0, 0-1, 0-2, and 0-3 transitions, respectively, comprising vibrational progression of the σ_4 mode of HC_9N for collective stretching motions of the carbon chain. Increments between adjacent pairs of bands are 2146, 2135, and 2115 cm^{-1}, in excellent agreement with the 1-0 fundamental for the σ_4 mode in the electronic ground state as observed at 2141 cm^{-1} in the IR and Raman spectra in Fig. 2 (see also Table 2). The major bands in the dispersed phosphorescence spectra of HC_9N in solid acetonitrile are listed in Table 3.

Figure 3.

Table 3.

The three spectra in Fig. 3a show peaks at the same wavelengths but with different intensities upon the different wavelength excitations. They are grouped into three series of progressions, namely A, B, and C. In Fig. 3b, the top trace in Fig. 3a is reproduced as a function of wavenumber, cm^{-1}, after subtraction of a featureless background. An intense peak in each 0-v band (v = 0-4), indicated as A, is accompanied by broader peaks at lower energies, indicated as B and C. The separation of the peak B from the peak A increases as 335, 346, 356, and 370 cm^{-1} as the vibrational progression of the σ_4 mode increases from v = 0 to v = 1, 2, and 3. The same trend is confirmed for the peak C. This trend is not compatible with the anharmonicity behavior of a vibrational mode. Moreover, relative intensity of the three peaks, A, B, and C, drastically changes for the different excitation energies as shown in Fig. 3a. These observations indicate that HC_9N molecules in solid acetonitrile are accommodated in three types of trapping sites where spatial arrangement of surrounding CH_3CN molecules are distinctly different for Site A, Site B and Site C. The phosphorescence peaks for Site A are as sharp as those reported in a solid Ar or Kr matrix [12].

To see the difference of the spectral features, A, B, and C, in more detail, Fig. 4 illustrates phosphorescence excitation mapping for the 0-0 band of HC_9N in solid

acetonitrile at 20 K. The two-dimensional (2D) contour plot in colors depicts emission intensity as functions of the emission and excitation wavelengths. Horizontal cross sections provide dispersed phosphorescence spectra as shown atop the 2D-map for selected excitation wavelengths of 241, 245, and 271 nm, for which the emission intensities at 582.3, 593.9, and 598.7 nm are the maximum for the peaks A, B, and C, respectively. Vertical cross sections constitute phosphorescence excitation spectra as shown to the right of the 2D-map for selected emission wavelengths for the relevant peaks A, B, and C. In the 2D-map, four major spots are vertically aligned along each line of the emission wavelengths at 582.3 nm for A, 593.9 nm for B, and 598.7 nm for C. This 4-band pattern shifts down on the map (red-shifts) when the detection wavelength changes in the direction from A to C. The mapping pattern clearly shows one-to-one correspondence between an emission peak and an excitation profile and is rationalized again by the presence of three distinct types of trapping sites for HC_9N molecules in solid acetonitrile.

Figure 4.

Note here that the excitation at 271 nm gives rise to the phosphorescence emission almost uniquely from Site C. This selective excitation is possible when the HC_9N molecule in a specific Site C has substantial absorption efficiency for the low energy UV photon relative to the molecule in the other Site A or B. The above mentioned red-shifts both in the excitation and emission energies indicate that energy gaps between the electronic ground state and the singlet/triplet excited states get smaller from A to C. A larger gap or a larger transition energy for A indicates the preferential stabilization of the ground-state HC_9N molecules in Site A. Conversely, the HC_9N molecules in Site B and C are relatively destabilized for the ground state.

Table 4 compiles minor features observed in Figs. 3 and 4, namely satellite peaks and shoulders in the phosphorescence of HC_9N in solid acetonitrile. In Fig. 3a, a satellite peak at 583.4 nm next to the main peak of Site A at 582.3 nm is as sharp as the main peak and red-shifted by ≈30 cm^{-1} from the main peak. The intensity of the satellite peak relative to the main peak increases from v = 0 to v = 1 and 2 for 0-v bands in the σ_4 progression. Moreover, in the mapping in Fig. 4, the maximum excitation wavelength

for the satellite peak "a" is downshifted by ≈1 nm (≈170 cm^{-1}) from that for the main peak "A". Furthermore, the appearance of this satellite peak resembles to the appearance of the secondary peak in the literature, which is well resolved in the solid Ar and Kr matrix hosts and assigned to HC_9N molecules trapped in a secondary matrix site [12]. Another satellite locating at higher energy is separated by 78 - 97 cm^{-1} from the main peak A for 0-v bands (v = 0-2) in the σ_4 progression. Having the same maximum excitation wavelength with the main peak A, this satellite is associated with a modification of the trapping site A. For peaks with such minute energy differences as less than ≈100 cm^{-1}, presence of an isotopolog, $H^{13}C^{12}C_8N$ (a total ≈9%, *i.e.*, ≈1% for each of the nine isotopomers), and corresponding zero-point-energy differences may also be subjects for considerations [29-31].

Table 4.

Concerning weak bands at 611.4 nm (1.635×10^4 cm^{-1}) and 617.6 nm (1.619×10^4 cm^{-1}) in Fig. 3a, dim spots in the mapping in Fig. 4 are relevant. The former shares the excitation maximum at 245 nm for B, while the latter shares the excitation maximum at 247 nm for C. Difference frequencies from the corresponding major bands are 482 cm^{-1} for B and 510 cm^{-1} for C, which are assignable to the π_4-bending fundamental [12].

Figure 5 shows scanned excitation spectra of HC_9N, obtained with the measurement mode (3), by motoring the emission intensity at 582.3 nm for A, 593.9 nm for B, and 598.7 nm for C. The strongest band peaking at 240.7 nm for A shifts to the red at 244. 9 nm for B. The other bands for B are shifted also to longer wavelengths compared to those for A. UV absorption spectrum of the solution of HC_9N in acetonitrile is shown for comparison (dashed line). Dotted lines are the excitation spectra obtained with the measurement mode (2) as reproduced from the right panel in Fig. 4 with vertical scaling. Peak positions and band widths are fitting well with the spectra between the mode (2) and (3), except for the spectral features in the dotted line spectrum for C, *i.e.*, peaks at 247, 258, and 271 nm. In Site C, the trapping environment for the HC_9N molecule can be modified to get stronger absorption efficiency for these excitation wavelengths, which might be developed under the long-term repetitive excitation cycle for the phosphorescence-mapping measurement.

Figure 5.

Figure 6a shows phosphorescence excitation mapping and a typical dispersed phosphorescence spectrum of HC_9N in solid *n*-hexane at 20 K. Within a relatively wide spectral range of 560 - 820 nm, three phosphorescence bands of the vibrational σ_4 progression are covered in one frame. The major bands in the dispersed phosphorescence spectra of HC_9N in *n*-hexane are listed in Table 3. The 2D contour plot shows some asymmetric red spots along each of the vertical lines for the 0-0, 0-1, or 0-2 bands. Each spot is elongated from up-left to down-right. In contrast to the spots in acetonitrile in Fig. 4, the phosphorescence features in *n*-hexane are not clearly resolved to be classified as distinct matrix sites. Nevertheless, as plotted in Fig. 6b, phosphorescence excitation spectra exhibit spectral features corresponding to absorption bands in the solution of *n*-hexane (dashed line in blue). In Table 1, observed bands in the phosphorescence excitation spectra of HC_9N in solid *n*-hexane in Fig. 6 as well as those in solid acetonitrile in Fig. 5 are listed for comparison with absorption features in solutions and with phosphorescence excitation peaks observed in the solid krypton matrix host [12].

Figure 6.

A difference to be noted here is that the spectral feature at ≈255 nm is not clearly discernible for the UV absorption in liquid acetonitrile and for the phosphorescence excitation in solid acetonitrile (Site A). However, peak positions as a whole by the phosphorescence excitation of HC_9N in solid *n*-hexane are not much different from those in solid acetonitrile (dotted line) and UV absorption bands in liquid acetonitrile (dashed line in purple) [17], bearing resemblance to a better resolved and consequently more complicated spectrum measured in solid krypton [12]. Phosphorescence excitation spectra are more complex than absorption spectra. It is because, at low temperatures, each of the single vibronic bands gets narrower and becomes well resolved, in contrast to blurred bands overlapping in a solution. In addition, the presence of multiple trapping sites makes the spectrum more complex in solid matrix hosts, whereas spectral details are obscured in solutions by averaging over a variety of instantaneous orientations of surrounding molecules.

Comparing the phosphorescence excitation with the UV absorption in more detail, the low energy part is more intense in excitation than in absorption for both acetonitrile in Fig. 5 and *n*-hexane in Fig. 6b. For the spectral region of 200 - 285 nm, multiple transitions are predicted from the ground state, $\tilde{X}^1\Sigma^+$, to several electronic excited states, $\tilde{D}^1\Delta$, $\tilde{E}^1\Sigma^+$, $\tilde{F}^1\Sigma^-$, $\tilde{G}^1\Delta$, $\tilde{H}^1\Sigma^+$ [12]. Among them, transitions to the $^1\Sigma^+$ states, $\tilde{E}$ (f = 2.8) and $\tilde{H}$ (f = 1.7), are fully allowed by the electric dipole mechanism, while transitions to the other $^1\Sigma^-$ and $^1\Delta$ states are forbidden but getting allowed via Herzberg-Teller coupling [32-34] with activation or deactivation of a π-symmetry vibration [12]. For symmetry forbidden singlet-singlet transitions of centrosymmetric polyyne molecules, $H(C{\equiv}C)_nH$, the mechanism of intensity borrowing and the type of inducing modes are discussed in some details [35]. In the cryogenic solid matrix hosts where the surrounding solvent molecules are tightly packed and their orientations are fixed, the electrostatic field in a trapping site for the target molecule can be anisotropic, which may break the symmetry selection rule. Accordingly, vibronic transitions via Herzberg-Teller coupling are promoted to be observed more intense than in solutions.

The structure in excitation shown in Figs. 4 and 5 for acetonitrile and in Fig. 6b for *n*-hexane has some similarities with the excitation spectrum in Fig. 7 in Ref. 12 for solid krypton. The low energy part shows a vibronic structure different from that of the high energy part, in agreement with the assignment to multiple excited states [12]. In particular, the spectral feature at 255 nm observed in *n*-hexane both for UV absorption (shoulder) and phosphorescence excitation (peak) could correspond to the band at 252.5 nm observed in solid Kr [12], which was difficult to include in a vibronic progression.

C. Phosphorescence of $HC_{11}N$

Figure 7 shows a typical phosphorescence spectrum of $HC_{11}N$ in solid acetonitrile at 20 K. With the excitation at 267.0 nm (solid line), three peaks at 643.7, 745.8, and 881.7 nm are conspicuous for vibronic 0-0, 0-1, and 0-2 transitions, respectively, in the $\tilde{a}^3\Sigma^+ \rightarrow \tilde{X}^1\Sigma^+$ system. These peaks are very weak at the excitation of 281.0 nm (dotted line), while the broad bands toward the low energy side are observed relatively strongly. The vibrational progression is due to excitation of the stretching σ_6 mode of $HC_{11}N$.

Increment between the 0-0 and 0-1 bands, 2108 cm^{-1}, is in very good agreement with the strong IR and Raman mode signal of σ_6 at 2105 cm^{-1} in Fig. 2. The narrow lines and the relevant broad bands are both belonging to $HC_{11}N$ and indicative of different trapping sites. The peaks in the dispersed phosphorescence spectra of $HC_{11}N$ in solid acetonitrile are listed in Table 3.

Figure 7.

By monitoring the phosphorescence intensity at 644 nm (0-0), the excitation wavelength is scanned continuously to obtain the excitation spectrum in Fig. 8. The action spectrum (solid line) of this measurement mode (3) is in good agreement with the absorption spectrum in the solution (dotted line), showing relatively narrow band shapes near the peak maxima. The bands in the phosphorescence excitation spectrum of $HC_{11}N$ in solid acetonitrile are listed in Table 1 for comparison with the UV absorption bands.

Figure 8.

For more details, a series of emission spectra of an expanded portion around the phosphorescence 0-0 band at 644 nm are recorded repeatedly during the scan of the excitation wavelength in a range of 213 - 302 nm by the mode (2) and plotted in Fig. 9 (left panel). From top to bottom, the characteristic cycle is observed several times, with a broad band that appears at shorter wavelength, shifts to longer wavelength, and fades. The observation is rationalized by the idea that a $HC_{11}N$ molecule absorbing a high (low) energy UV photon emits a high (low) energy visible photon as phosphorescence. This trend is seen more clearly in the phosphorescence excitation mapping in Fig. 9 (right panel), *i.e.*, several bumps tailing from up-left to down-right, each of which corresponds to the UV absorption band (*c.f.* dotted line in Fig. 8).

Figure 9.

The most significant feature of the phosphorescence mapping in Fig. 9 is the narrow peak at 644 nm on top of the broad band, which does not shift by the excitation wavelength. The upper state of the emission, $\tilde{a}^3\Sigma^+$, as well as the lower state, $\tilde{X}^1\Sigma^+$, is populated as a well-defined state in the matrix host. This phenomenon is explainable by

Shpolsky effects [36], where the host molecules are crystallized around the guest molecule, providing a unique matrix environment of a single trapping site. When the action spectrum of the excitation is deduced only from the areal magnitude of the narrow peak at 644 nm, for which the contribution from the broad band below the peak is subtracted, the spectrum shows narrow peaks also in the excitation spectrum as in Fig. 10. Major high energy bands exhibit relatively narrow peaks, although two low energy bands are relatively broad. However, increments between adjacent peaks from low energy are 1724, 1723, 1881, and 1812 cm^{-1}, being irregular and even increasing in energy. This is not compatible with the idea for assigning them to a single vibrational mode progression in a single electronic potential surface. Moreover, it is apparent from Table 1 that the absorption bands of $HC_{11}N$ readily show the same irregularity. This is because of still unresolved vibronic features even under the condition of cryogenic matrix experiments. As is demonstrated in the excitation spectrum of matrix isolated HC_9N molecules in cryogenic solid krypton [12], the excitation spectra as well as the absorption spectra are constituted intrinsically by more complex vibronic features due to the effects by strong intensity borrowing between many electronic states.

Figure 10.

D. Phosphorescence lifetimes

Phosphorescence lifetimes were measured by temporal decay profiles of the emission intensity. Several bands at particular excitation and emission wavelengths were examined to realize that the decay constant is more or less the same for the same molecule, indicating that the observed lifetime reflects the population decay of the lowest triplet state, $\tilde{a}^3\Sigma^+$. The observed lifetimes at 20 K with fitting error bars are 11.2 ± 0.1 ms in acetonitrile and 9.7 ± 0.1 ms in *n*-hexane for HC_9N and 7.6 ± 0.1 ms in acetonitrile for $HC_{11}N$. For HC_9N, the slightly shorter lifetime in *n*-hexane than that in acetonitrile may be attributable to the larger number of vibrational degrees of freedom for the host *n*-hexane molecules, leading to enhanced energy dissipation. Although several milliseconds deviations are admitted from different settings for the termination resistance in the measurement system, a clear trend is confirmed that the longer

cyanopolyyne, $HC_{11}N$, has a shorter lifetime than HC_9N. This is in good agreement with the trend for reported lifetimes of 40 ms for HC_5N, 8.2 ms for HC_7N and 3.9 ms for HC_9N in solid Kr matrices [10,12].

E. Transition energies and the molecular size

Figure 11 summarizes the experimental transition wavelengths of the phosphorescence 0-0 band for cyanopolyynes $HC_{2n+1}N$ (n = 2-5) as a function of the size of the conjugated linear carbon chain, *i.e.*, the number of carbon atoms in a molecule. The UV absorption maxima of cyanopolyynes $HC_{2n+1}N$ (n = 3-6) and hydrogen-capped polyynes $C_{2n}H_2$ (n = 3-7) are plotted for reference. Both types of transitions in the visible and UV regions show a systematic trend proportional to the molecular size, as expected for the particle-in-a-box model. The upper state of the phosphorescence, $\tilde{a}^3\Sigma^+ \rightarrow \tilde{X}^1\Sigma^+$, stems from the same electron configuration as the upper state of the lowest-energy fully-dipole-allowed transition, $^1\Sigma^+ \leftarrow \tilde{X}\,^1\Sigma^+$, but differs in the spin state. The HOMO-LUMO excitation (π-π^*) provides three excited states, Σ^+, Σ^-, and Δ [12,35]. Among the three, the upper state for the fully allowed transition, $^1\Sigma^+$, locates at the highest energy and the other two, $^1\Sigma^-$ and $^1\Delta$, come to the lowest excited energy within the singlet manifold. For the symmetry forbidden transition to the $^1\Delta$ state from the $\tilde{X}^1\Sigma^+$ ground state, Herzberg-Teller coupling with a vibrational π-mode excitation is crucial. The lowest energy triplet state for the phosphorescence, $\tilde{a}^3\Sigma^+$, locates slightly lower than the lowest energy singlets, thus the phosphorescence excitation measurement for the $^1\Delta$ state is possible [12]. The vibronic structure in the phosphorescence excitation spectrum for the $^1\Delta \leftarrow \tilde{X}^1\Sigma^+$ transition is much simpler than the structure for the fully allowed $^1\Sigma^+ \leftarrow \tilde{X}^1\Sigma^+$ transition.

Figure 11.

Since the upper state of the former is remote in energy from the upper state of the fully allowed transition, the transition occurs simply within a single pair of the upper and lower electronic states, even though the Herzberg-Teller coupling is required [12,32-34]. In contrast, the fully allowed transition of the latter occurs with numerous vibronic

transitions to a number of nearby electronic states to which the intensity borrowing from the fully allowed transition is heavily promoted, *i.e.*, the oscillator strength of the fully allowed transition is distributed to the other electronic transitions having overlapping vibronic levels in the vicinity. In this type of strongly coupled plasmonic transitions, the vibronic intensity is not simply governed by usual Franck-Condon factors between the two electronic states and even the origin band is not easily located [37].

Summary

Two cyanopolyyne molecules, HC_9N and $HC_{11}N$, were isolated from solutions of laser-ablated graphite particles in acetonitrile and UV absorption spectra were recorded in acetonitrile and *n*-hexane. IR absorption spectra were measured in CCl_4, while UV resonance Raman spectra were observed in *n*-hexane. Appearing both in the IR and Raman spectra in a range of 2030 - 2240 cm^{-1}, five modes in HC_9N, σ_2 - σ_6, and five modes in $HC_{11}N$, σ_2 - σ_7 except for σ_4, were identified as stretching vibrational modes of the sp-hybridized $–(C\equiv C–)_nC\equiv N$ chain. Phosphorescence signals appearing at 582.3 nm (0-0), 665.4 nm (0-1), and 775.6 nm (0-2), and 927.8 nm (0-3) in the solid acetonitrile matrix host constitute vibrational progression of the stretching σ_4 mode in the electronic ground state of HC_9N, fairly consistent with the vibrational frequency of 2141 cm^{-1} by the IR and Raman measurement. For $HC_{11}N$, phosphorescence signals were peaking at 643.7 nm (0-0), 744.8 nm (0-1), and 881.7 nm (0-2), consistent with the σ_6 fundamental of 2105 cm^{-1} in the IR and Raman spectra. Phosphorescence excitation mapping showed UV absorption dynamics in the cryogenic solids of organic molecules explainable by the presence of multiple trapping sites as well as crystalline sites with sharp emission/absorption features by Shpolsky effects, *i.e.*, the three distinct trapping sites for HC_9N in solid acetonitrile in particular. Vibronic patterns of the UV excitation were found irregular which highlight the multiple electronic excited states involved. Phosphorescence lifetimes were longer for HC_9N than that for $HC_{11}N$.

Acknowledgments

The MEXT-Supported Program for the Strategic Research Foundation at Private Universities for Establishing a Best-Energy-Mix Research Center to Promote the Use of Solar Energy subsidized from the Ministry of Education, Culture, Sports, Science and Technology of Japan (MEXT) and Kindai University is greatly acknowledged. US is supported by the Mobility Contest Internship Program, Institute of Physical Chemistry, Polish Academy of Sciences for collaboration performed at Kindai University.

Supplementary data

Calculated IR and Raman data are provided as supplementary Table S1 with their plots in spectra in Figs. S1 (IR) and S2 (Raman) for HC_9N and $HC_{11}N$. Molecular orbital (MO) calculations were performed at the B3LYP level of density functional theory (DFT) with various basis sets using M. J. Frisch *et al.*, *Gaussian* 16, Revision A.03, Gaussian Inc. Wallingford, CT, 2016. The calculated harmonic frequencies are scaled by 0.967 for anharmonicity corrections.

References

[1] N.W. Broten, T. Oka, L.W. Avery, J.M. MacLeod, H.W. Kroto, The detection of HC_9N in interstellar space, Astrophys. J. 223 (1978) L105.

[2] R.L. Snell, F.P. Schloerb, J.S. Young, A. Hjalmarson, P. Friberg, Observations of HC_3N, HC_5N, and HC_7N in molecular clouds, Astrophys. J. 244 (1981) 45-53.

[3] M.B. Bell, L.W. Avery, J.M. MacLeod, H.E. Matthews, The excitation temperature of HC_9N in the circumstellar envelope of IRC +10216, Astrophys. J. 400 (1992) 551-555.

[4] Truong-Bach, D. Graham, Nguyen-Q-Rieu, HC_9N from the Envelopes of IRC+10216 and CRL:2688, Astron. Astrophys. 277 (1993) 133.

[5] R.A. Loomis, C.N. Shingledecker, G. Langston, B.A. McGuire, N.M. Dollhopf, A.M. Burkhardt, J. Corby, S.T. Booth, P.B. Carroll, B. Turner, A.J. Remijan,

Non-detection of $HC_{11}N$ towards TMC-1: Constraining the chemistry of large carbon-chain molecules, Mon. Not. R. Astron. Soc. 463 (2016) 4175-4183.

[6] K.M.T. Yamada, M. Bester, M. Tanimoto, G. Winnewisser, Pure rotational spectrum of cyanopropyne in the v_{12} = 1 vibrational state, J. Mol. Spectrosc. 126 (1987) 118-128.

[7] A. Coupeaud, R. Kołos, I. Couturier-Tamburelli, J.P. Aycard, N. Piétri, Photochemical Synthesis of the Cyanodiacetylene HC_5N: A Cryogenic Matrix Experiment, J. Phys. Chem. A 110 (2006) 2371-2377.

[8] C. Crépin, M. Turowski, J. Ceponkus, S. Douin, S. Boyé-Péronne, M. Gronowski, R. Kołos, UV-Induced growth of cyanopolyyne chains in cryogenic solids, Phys. Chem. Chem. Phys. 13 (2011) 16780-16785.

[9] I. Couturier-Tamburelli, N. Piétri, C. Crépin, M. Turowski, J.-C. Guillemin, R. Kołos, Synthesis and spectroscopy of cyano-triacetylene (HC_7N) in solid argon, J. Chem. Phys. 140 (2014) 044329.

[10] M. Turowski, C. Crépin, M. Gronowski, J.-C. Guillemin, A. Coupeaud, I. Couturier-Tamburelli, N. Piétri, R. Kołos, Electronic absorption and phosphorescence of cyanodiacetylene, J. Chem. Phys. 133 (2010) 074310.

[11] M. Turowski, C. Crépin, S. Douin, M. Gronowski, I. Couturier-Tamburelli, N. Piétri, A. Wasiak, R. Kołos, Low temperature Raman spectra of cyanobutadiyne (HC_5N), Vib. Spectrosc. 62 (2012) 268-272.

[12] U. Szczepaniak, C. Crépin, M. Gronowski, M. Chevalier, J.-C. Guillemin, M. Turowski, T. Custer, R. Kołos, Cryogenic photochemical synthesis and electronic spectroscopy of cyanotetraacetylene. J. Phys. Chem. A 121 (2017) 7374-7384.

[13] U. Szczepaniak, M. Turowski, T. Custer, M. Gronowski, N. Kerisit, Y. Trolez, R. Kołos, Infrared and Raman spectroscopy of methylcyanodiacetylene (CH_3C_5N), ChemPhysChem 17 (2016) 3047-3054.

[14] U. Szczepaniak, R. Kołos, M. Gronowski, M. J.-C. Guillemin, C. Crépin, Low temperature synthesis and phosphorescence of methyltriacetylene, J. Phys. Chem. A 122 (2018) 89-99.

[15] M. Turowski, U. Szczepaniak, T. Custer, M. Gronowski, R. Kołos, Electronic spectroscopy of methylcyanodiacetylene (CH_3C_5N), ChemPhysChem 17 (2016) 4068-4078.

[16] H. Tabata, M. Fujii, M. Hayashi, T. Doi, T. Wakabayashi, Raman and surface-enhanced Raman scattering of a series of polyynes, Carbon 44 (2006) 3168-3176.

[17] T. Wakabayashi, M. Saikawa, Y. Wada, T. Minematsu, Isotope scrambling in the formation of cyanopolyynes by laser ablation of carbon particles in liquid acetonitrile, Carbon 50 (2012) 47-56.

[18] T. Wakabayashi, H. Tabata, T. Doi, H. Nagayama, K. Okuda, R. Umeda, I. Hisaki, M. Sonoda, Y. Tobe, T. Minematsu, K. Hashimoto, S. Hayashi, Resonance Raman spectra of polyyne molecules $C_{10}H_2$ and $C_{12}H_2$ in solution, Chem. Phys. Lett. 433 (2007) 296-300.

[19] T. Wakabayashi, H. Nagayama, K. Daigoku, Y. Kiyooka, K. Hashimoto, Laser induced emission spectra of polyyne molecules $C_{2n}H_2$ (n=5-8), Chem. Phys. Lett. 446 (2007) 65-70.

[20] Y. Wada, Y. Morisawa, T. Wakabayashi, Spectroscopic characterization of a series of polyyne-iodine molecular complexes $H(C{\equiv}C)_nH(I_6)$ of n=5-9, Chem. Phys. Lett. 541 (2012) 54-59.

[21] D. Nishide, H. Dohi, T. Wakabayashi, E. Nishibori, S. Aoyagi, M. Ishida, S. Kikuchi, R. Kitaura, T. Sugai, H. Shinohara, Single-wall carbon nanotubes encaging linear chain $C_{10}H_2$ polyyne molecules inside, Chem. Phys. Lett. 428 (2006) 356-360.

[22] D. Nishide, T. Wakabayashi, H. Kataura, Y. Achiba, H. Shinohara, Raman spectroscopy of size-selected linear polyyne molecules $C_{2n}H_2$ (n = 4-6) encapsulated in single-wall carbon nanotubes, J. Phys. Chem. C 111 (2007) 5178-5183.

[23] T. Wakabayashi, T. Murakami, H. Nagayama, D. Nishide, H. Kataura, Y. Achiba, H. Tabata, S. Hayashi, H. Shinohara, Raman spectral features of longer polyynes $HC_{2n}H$ (n = 4-8) in SWNTs, Eur. Phys. J. D 52 (2009) 79-82.

[24] R. Sata, H. Suzuki, N. Ueno, Y. Morisawa, M. Hatanaka, T. Wakabayashi, UV-polarizing linear polyyne molecules aligned in PVA, Chin. J. Chem. Phys. 32 (2019) 175-181.

[25] Z. Mielke, A. Olbert-Majkut, K. G. Tokhadze, Photolysis of the OC···HONO complex in low temperature matrices: Infrared detection and *ab initio* calculations of nitrosoformic acid, HOC(O)NO, J. Chem. Phys. 118 (2003) 1364-1377.

[26] Z. Mielke, S. Coussan, K. Mierzwicki, P. Roubin, M. Sałdyka, The complex between CH3OH and CF4. Infrared matrix isolation and theoretical studies, J. Phys. Chem. A 110 (2006) 4712-4718.

[27] M. Sałdyka and Z. Mielke, The interaction of formohydroxamic acid with nitrogen: FTIR matrix isolation and ab initio studies, J. Mol. Struct. 708 (2004) 183-188.

[28] R. Eastmond, T. R. Johnson, D. R. M. Walton, Silylation as a protective method for terminal alkynes in oxidative couplings - A general synthesis of the parent polyynes $H(C{\equiv}C)_nH$ (n = 4-10, 12), Tetrahedron 28 (1972) 4601-4616.

[29] T. Wakabayashi, T. Momose, M. E. Fajardo, Matrix isolation spectroscopy and spectral simulations of isotopically substituted C_{60} molecules, J. Chem. Phys. 151 (2019) 234301.

[30] H. Hoshina, T. Wakabayashi, T. Momose, T. Shida, Infrared spectroscopic study of rovibrational states of perdeuterated methane (CD_4) trapped in parahydrogen crystal, J. Chem. Phys. 110 (1999) 5728-5733.

[31] T. Momose, H. Hoshina, N. Sogoshi, H. Katsuki, T. Wakabayashi, T. Shida, Tunneling chemical reactions in solid parahydrogen: A case of $CD_3 + H_2 \rightarrow CD_3H + H$ at 5 K, J. Chem. Phys. 108 (1998) 7334-7338.

[32] G. Orlandi and W. Siebrand, Theory of vibronic intensity borrowing. Comparison of Herzberg-Teller and Born-Oppenheimer coupling, J. Chem. Phys. 58 (1973) 4513-4523.

[33] S. H. Lin and H. Eyring, Study of vibronic and Born-Oppenheimer couplings, Proc. Nat. Acad. Sci. USA 71 (1974) 3415-3417.

[34] S. H. Lin and H. Eyring, Study of the Franck-Condon and Herzberg-Teller Approximations, Proc. Nat. Acad. Sci. USA 71 (1974) 3802-3804.

[35] T. Wakabayashi, Y. Wada, N. Iwahara, T. Sato, Vibronic bands in the HOMO-LUMO excitation of linear polyyne molecules, J. Phys: Conf. Ser. 428 (2013) 012004.

[36] A. V. Naumov, Low-temperature spectroscopy of organic molecules in solid matrices: from the Shpol'skii effect to laser luminescent spectroscopy for all effectively emitting single molecules, Phys. Usp. 56 (2013) 605-622 [Usp. Fiz. Nauk. 183 (2013) 633-652].

[37] G. Monninger, M. Förderer, P. Gürtler, S. Kalhofer, S. Petersen, L. Nemes, P. G. Szalay, W. Krätschmer, Vacuum ultraviolet spectroscopy of the carbon molecule

C_3 in matrix isolated state: Experiment and theory, J. Phys. Chem. 106 (2002) 5779-5788.

Table 1. UV absorption and phosphorescence excitation features of HC_9N and $HC_{11}N$.

Species	Absorption / nm		Phosphorescence Excitation / nm		
	Acetonitrile[a)]	*n*-Hexane[a)]	Acetonitrile[b)]	*n*-Hexane[b)]	Kr[c)]
HC_9N	201.3				210.4 [47,534]
	211.8	212.0			211.9 [47,201]
	221.6	221.0	223 (224)	222	218.7 [45,729] 221.0 [45,247]
	230.9	231.0	232 (235)	231	227.7 [43,921] 231.5 [43,189]
	238.8	238.8	240.7	241	237.3 [42,148] 238.2 [41,973]
	244.4	245.6	(244.9)		243.5 [41,070] 244.0 [40,986]
	248.9	248.6	249.6	250	248.4 [40,252]
		255.0	(255)	255	252.5 [39,605] 255.9 [39,085]
	260.3	261.0	263 (267)	262	260.1 [38,449] 260.7 [38,358]
	273.7	272.0	275 (278)	274	268.8 [37,201] 272.9 [36,647] 273.6 [36,554]
	288.3				283.4 [35,288] 288.1 [34,706] 289.0 [34,598]
$HC_{11}N$	212.8	212.0			
	222.2	222.2	224.25		
	232.1	232.0	233.75		
	242.0	242.2	244.50		
	253.3	253.3	255.25		
	264.5	264.4	263.25 267.00		
	274.5	273.6 284.0	275.75		
	289.2	287.0	289.75		
	304.9	303.8			
	321.8				

a) Solutions at ambient temperature [17].
b) Solid matrices at 20 K: Wavelengths in parenthesis are for Site B in solid acetonitrile (this work).
c) Solid Kr matrices: Wavenumbers in cm^{-1} in braces are reported in the literature [12].

Table 2. Observed IR and Raman peaks of HC_9N and $HC_{11}N$ in solutions.

Species	Frequency (cm^{-1})	Intensity[a)]		Mode	Assignment[g)]
	IR[b)]	IR[b)]	Raman[c)]		
HC_9N	3302	s.		σ_1	CH str.
	2239	m.	w.	σ_2	CN str.[h)]
	2190	vw.	vw.	σ_3	CC str.[i)]
	2174	w.	w.	$2\sigma_8$	
	2141	s.	s.	σ_4	
	2115	w.	w.	σ_5	
	2030	-	w.[d)]	σ_6	
	632	sh.		π_1	CH bend.
	626	s.			
$HC_{11}N$	3303	s.		σ_1	CH str.
	2235	m.	w.	σ_2	CN str.[h)]
	2184	vw.	-	σ_3	CC str.[i)]
	2139	w.	-	σ_5[e)]	
	2105	s.	s.	σ_6[e)]	
	2100			$\sigma_7 + 2\pi_{11}$	
	2085	w.	sh.	combination[f)]	
	2028	-	w.	σ_7	
	632	m.		π_1	CH bend.

a) Abbreviations: s. (strong), m. (medium), w. (weak), vw. (very weak), sh. (shoulder).
b) Solvent: CCl_4.
c) Solvent: *n*-hexane.
d) Overlapping with an impurity peak.
e) Strongly perturbed by overtones and combinations.
f) Candidates: $\sigma_9 + 4\pi_8$, $2\sigma_{11} + 2\pi_6$, or $\sigma_9 + \sigma_{10}$.
g) Abbreviations: str. (stretching), bend. (bending).
h) A collective mode with CC stretching motions.
i) Collective modes with the CN stretching motion.

Table 3. Major vibrational progression observed in the dispersed phosphorescence spectra of HC_9N and $HC_{11}N$ in cryogenic matrix hosts of solid organic molecules.

Species	Acetonitrile		*n*-Hexane		Assignment
	λ (nm)	Δ (cm^{-1})	λ (nm)	Δ (cm^{-1})	$\tilde{a}^3\Sigma^+ \rightarrow \tilde{X}^1\Sigma^+$
HC_9N	582.3		584		0_0^0 (0-0)
		2146		2131	
	665.4		667		4_1^0 (0-1)
		2135		2016	
	775.6		776		4_2^0 (0-2)
		2115			
	927.8		-		4_3^0 (0-3)
$HC_{11}N$	643.7		-		0_0^0 (0-0)
		2108			
	744.8		-		6_1^0 (0-1)
		2085			
	881.7		-		6_2^0 (0-2)

Table 4. Site peaks and satellite peaks in the phosphorescence spectra of HC_9N in solid acetonitrile at 20 K. Three distinct matrix sites are denoted by A, B, and C. Difference frequencies in cm^{-1} are relative to the main peak within the same group of 0-v bands (v = 0, 1, and 2) in the common site.

HC_9N Progression σ_4	Observed Peaks				Difference Frequencies		
	Appearance	Wavelength / nm			Wavenumber / cm^{-1}		
		A	B	C	A	B	C
0 - 0	satellite	579.6	-	-	–78	-	-
	shoulder	582.1	-	-	–4	-	-
	main peak	582.3	593.9	598.7	0	0	0
	satellite[a)]	583.4	-	-	32	-	-
	shoulder	584.7	-	600.2	72	-	42
	weak band[b)]	-	611.4	617.6	-	482	510
0 - 1	shoulder	660.6	-	-	–109	-	-
	satellite	661.8	-	-	–83	-	-
	shoulder	664.3	-	-	–24	-	-
	main peak	665.4	681.1	687.4	2146[c)]	2156[c)]	2155[c)]
	satellite[a)]	666.9	-	-	33	-	-
	shoulder	668.5	682.4	689.7	69	28	48
	weak band[b)]	-	703.8	710.9	-	473	480
0 - 2	satellite	769.8	-	-	–97	-	-
	shoulder	774.4	-	-	–20	-	-
	main peak	775.6	797.6	805.5	2135[d)]	2144[d)]	2132[d)]
	satellite[a)]	777.5	-	-	30	-	-
	shoulder	779.8	-	-	69	-	-
0 - 3	main peak	927.8	960.8	-	2115[e)]	2130[e)]	-

a) Split side-peaks in Fig. 3 and a down-shifted peak “a” in Fig. 4.
b) Assigned to $v\sigma_4 + \pi_4$ (v = 0, 1, and 2) as in Ref. 12.
c) Difference from the 0-0 main peak.
d) Difference from the 0-1 main peak.
e) Difference from the 0-2 main peak.

Figure Captions

Figure 1. UV absorption spectra of HC_9N and $HC_{11}N$ in solutions of *n*-hexane.

Figure 2. IR absorption spectra in CCl_4 (upper traces) and UV resonance Raman spectra in *n*-hexane (lower traces) of HC_9N and $HC_{11}N$ in solutions at ambient temperature. A peak with an asterisk is a Raman signal of impurity molecules.

Figure 3. Dispersed phosphorescence spectra of HC_9N in solid acetonitrile (CH_3CN) at 20 K. a) Spectra in nm at different excitation wavelengths of 250.0, 255.0, and 271.0 nm and b) the spectrum in cm^{-1} (background subtracted) at 250.0 nm excitation.

Figure 4. Phosphorescence mapping for HC_9N in solid acetonitrile at 20 K. Dispersed phosphorescence spectra by excitations at 241, 245, 271 nm (top). Excitation spectra by phosphorescence intensities at 582.3, 593.9, and 598.7 nm (right).

Figure 5. Phosphorescence excitation spectra of HC_9N in solid acetonitrile at 20 K plotted for intensities at A 582.3, B 593.9, and C 598.7 nm (mode 3). Dotted line spectra are reproduced from Fig. 4 with vertical scaling (mode 2). Dashed line is the UV absorption spectrum in a solution of acetonitrile at ambient temperature, for which circle markers indicate absorption features at 238.8, 244.4, and 248.9 nm. An asterisk indicates the artificial peak by SHG-crystal switching.

Figure 6. a) Phosphorescence mapping for HC_9N in solid *n*-hexane at 20 K. The trace in white is a dispersed phosphorescence spectrum by the excitation at 250 nm. b) Excitation spectra plotted by the phosphorescence intensity at indicated wavelengths. UV absorption spectra in *n*-hexane and acetonitrile at ambient temperature (dashed lines) and an excitation spectrum in acetonitrile in Fig. 4 (dotted line) are shown for comparison.

Figure 7. Phosphorescence spectrum of $HC_{11}N$ in solid acetonitrile at 20 K.

Figure 8. Phosphorescence excitation spectrum of $HC_{11}N$ in solid acetonitrile at 20 K by monitoring the intensity at 644 nm during the continuous UV wavelength scan. Dotted line shows absorption spectrum in the solution at ambient temperature.

Figure 9. Phosphorescence spectra (left panel) and their excitation mapping (right panel) for the 0-0 band of $HC_{11}N$ in solid acetonitrile at 20 K.

Figure 10. Phosphorescence excitation spectrum of $HC_{11}N$ in solid acetonitrile at 20 K by plotting the peak intensity at 644 nm in Fig. 9 for the Shpolsky site.

Figure 11. Phosphorescence transition wavelengths of the 0-0 band for cyanopolyynes $HC_{2n+1}N$ (n = 2-5) in solid Ar [9,10,12] and in solid acetonitrile (this work). UV absorption maxima in solutions are plotted for reference [16,17,28].

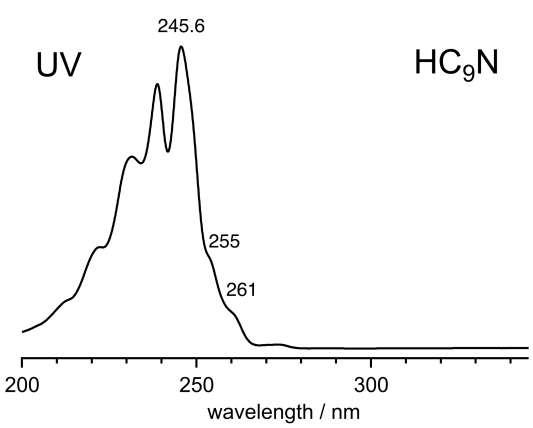

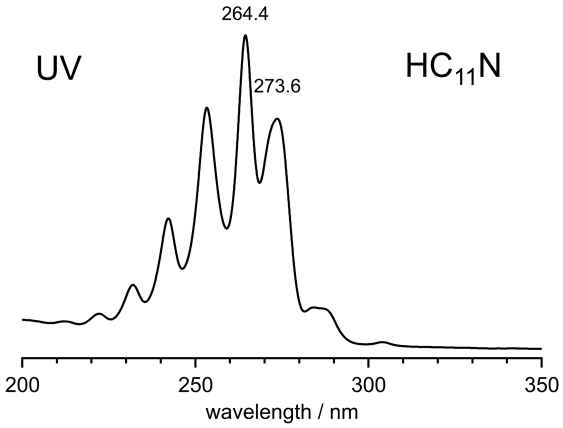

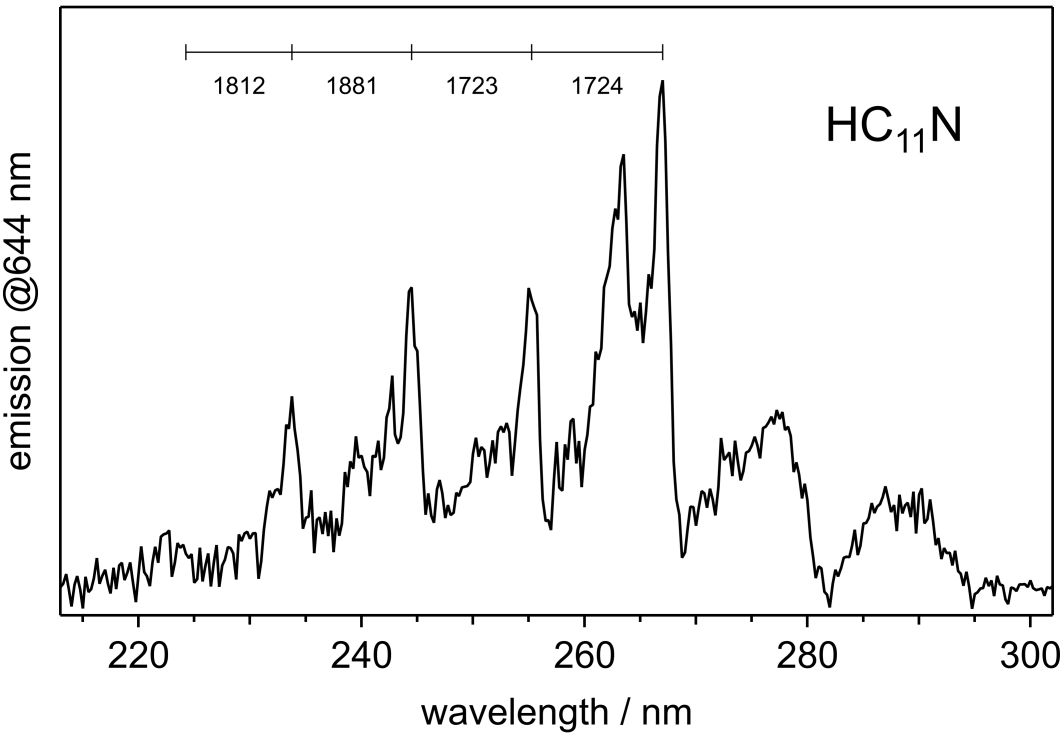

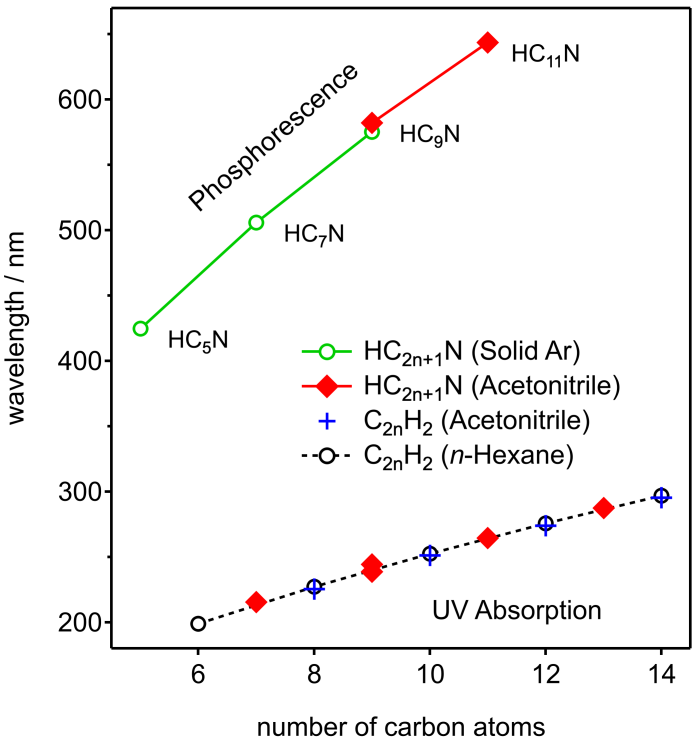

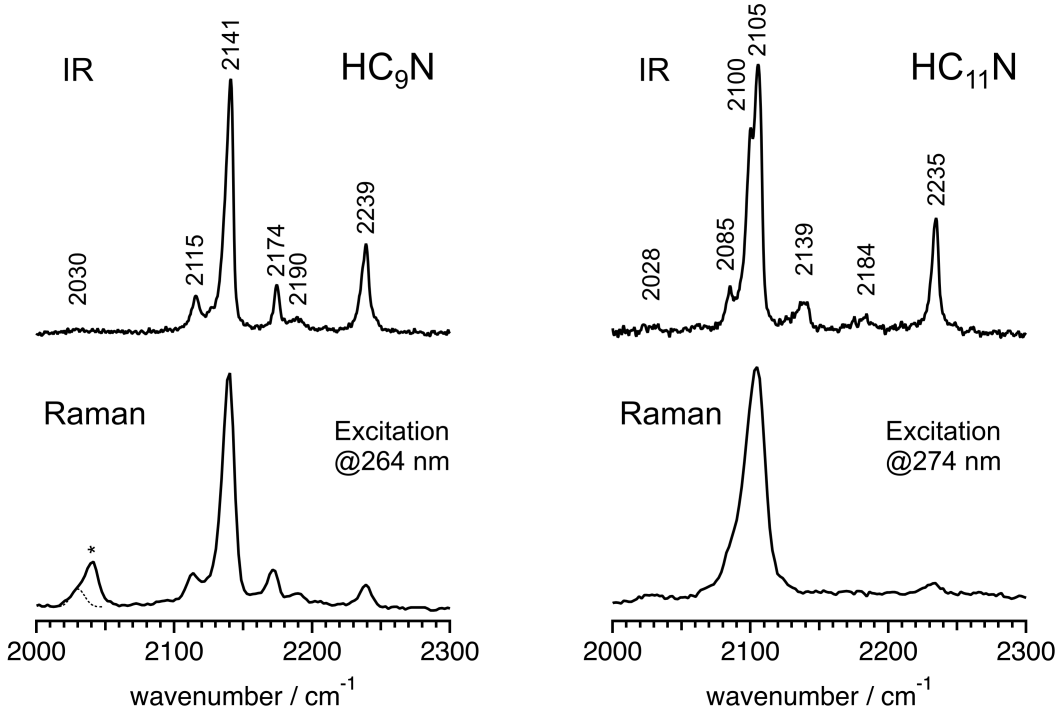

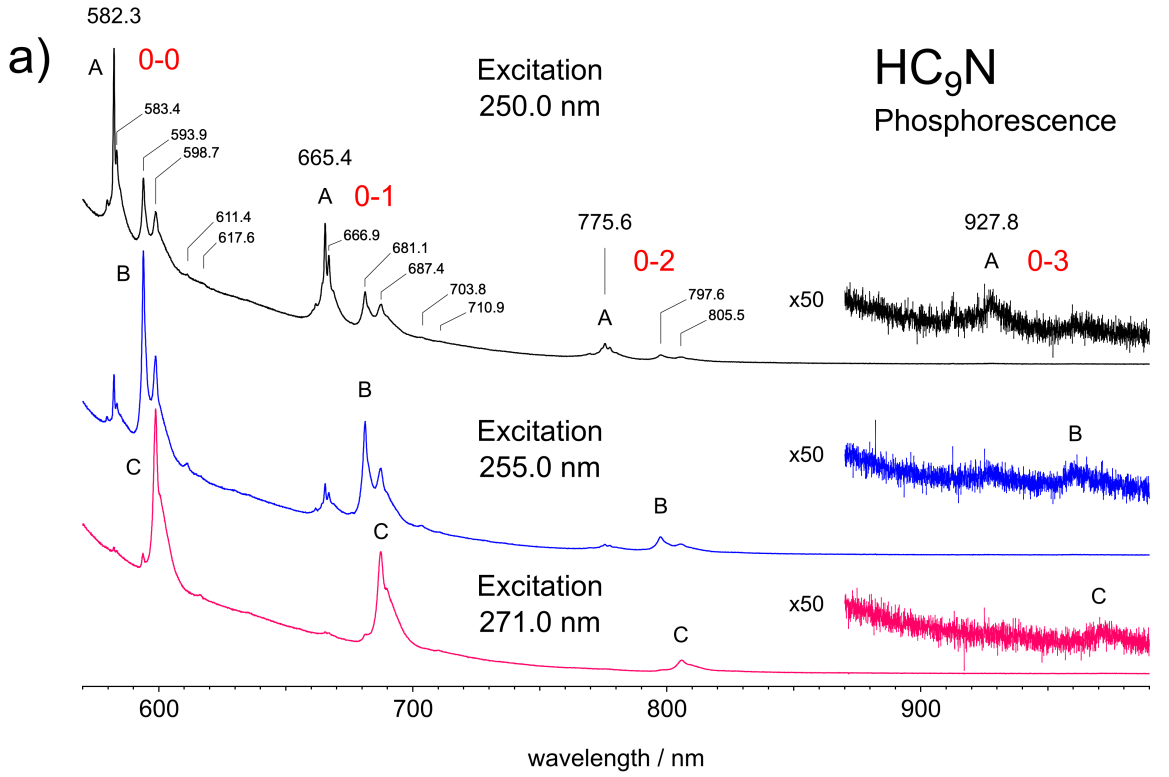
a)
582.3
A
0-0
583.4
593.9
598.7
611.4
617.6
665.4
A
0-1
666.9
681.1
687.4
703.8
710.9
775.6
0-2
797.6
805.5
927.8
A
0-3
x50
B
Excitation
250.0 nm
HC9N
Phosphorescence
C
Excitation
255.0 nm
Excitation
271.0 nm
600
700
800
900
wavelength / nm

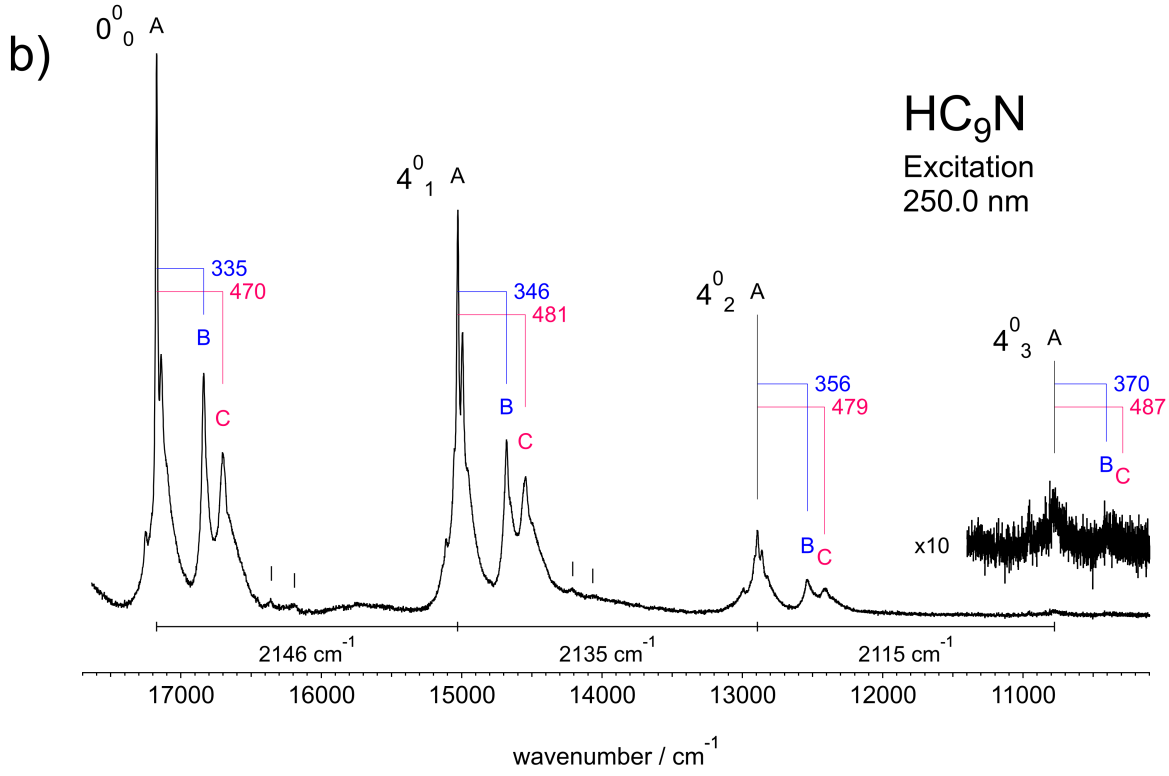
b)
0 0 0 A
4 0 1 A
4 0 2 A
4 0 3 A
335
470
346
481
356
479
370
487
B
C
x10
HC9N
Excitation
250.0 nm
2146 cm-1
2135 cm-1
2115 cm-1
17000
16000
15000
14000
13000
12000
11000
wavenumber / cm-1

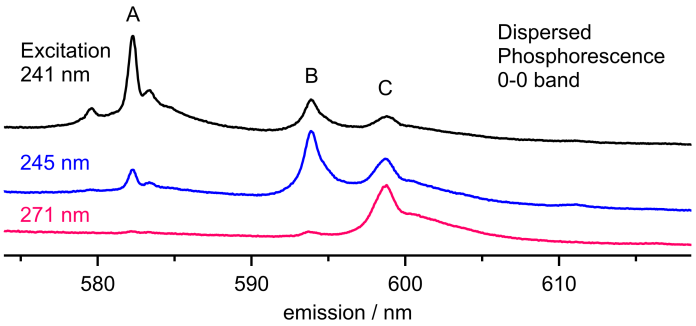

HC_9N

Phosphorescence in Acetonitrile (Solid@20 K)

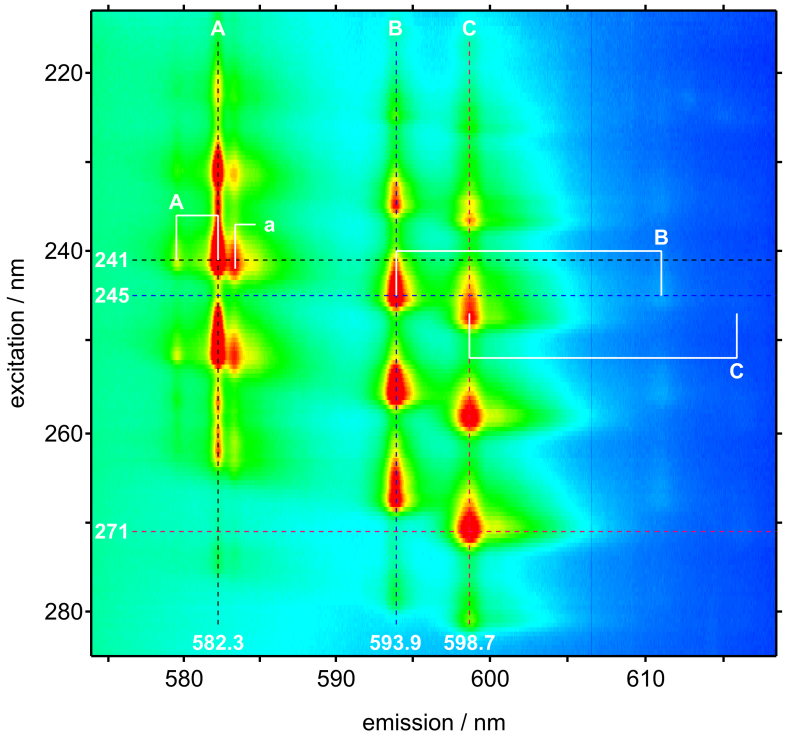

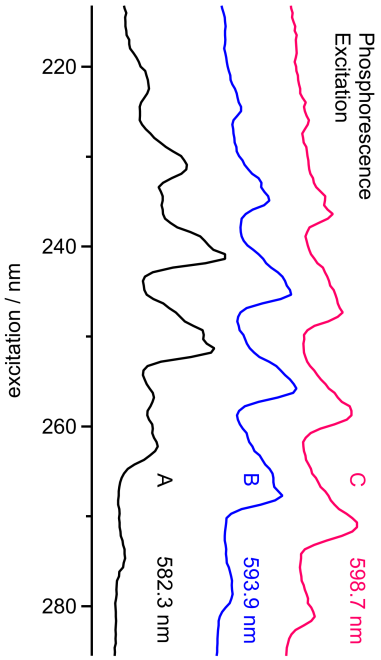

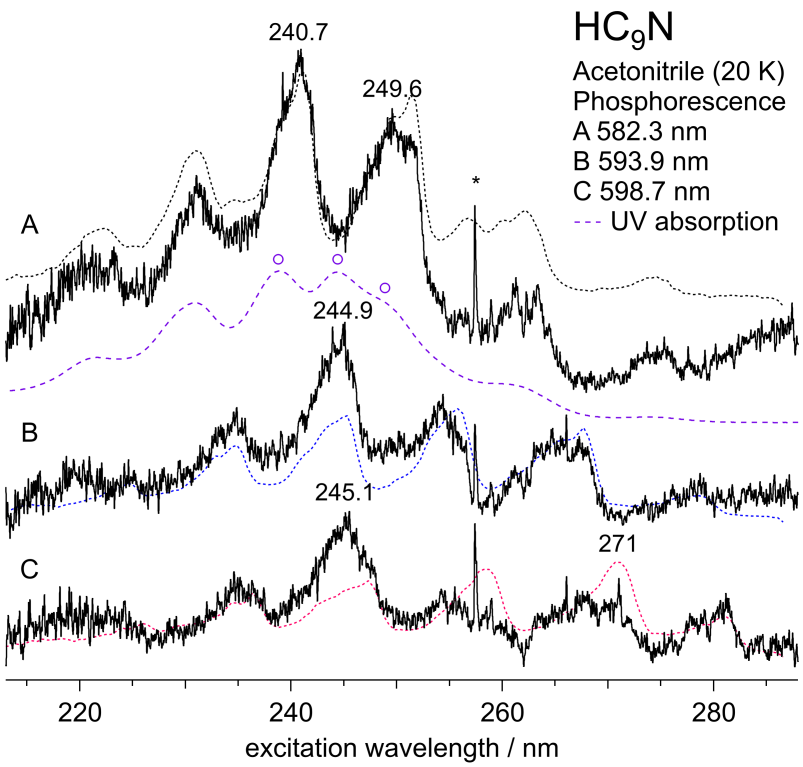

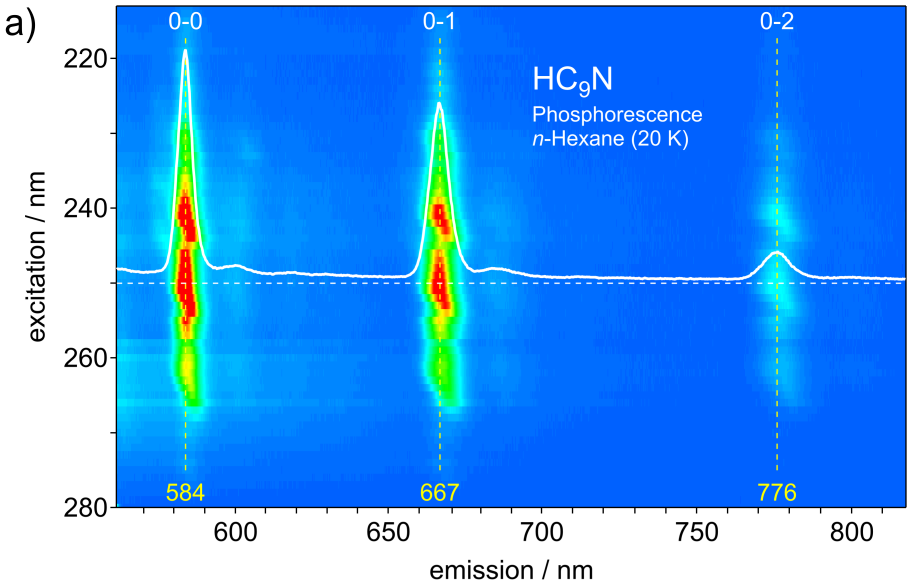
a)
0-0
0-1
0-2
HC9N
Phosphorescence
n-Hexane (20 K)
excitation / nm
220
240
260
280
584
667
776
600
650
700
750
800
emission / nm

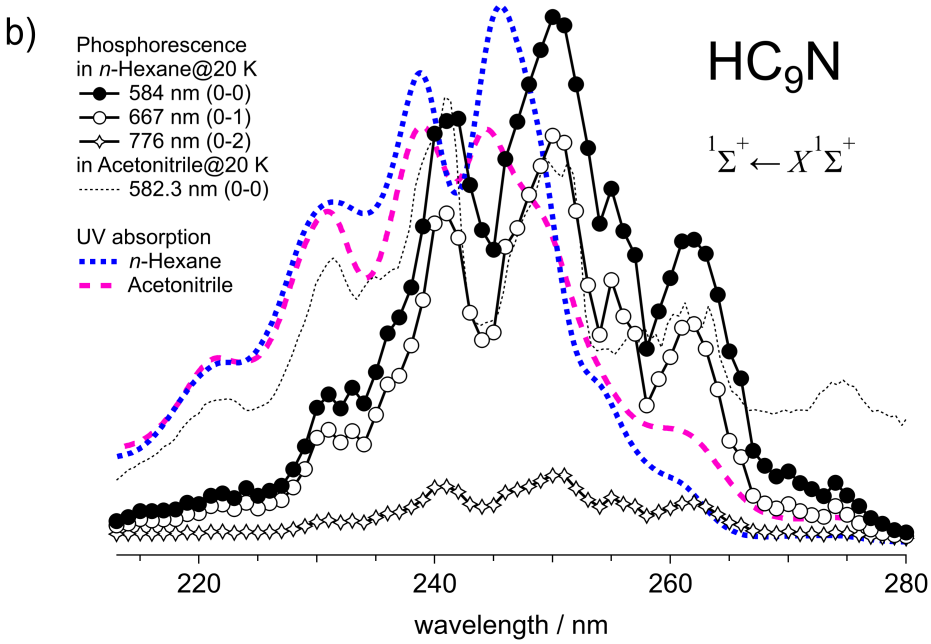
b)
Phosphorescence
in n-Hexane@20 K
584 nm (0-0)
667 nm (0-1)
776 nm (0-2)
in Acetonitrile@20 K
582.3 nm (0-0)
UV absorption
n-Hexane
Acetonitrile
HC9N
1Σ+ ← X 1Σ+
220
240
260
280
wavelength / nm

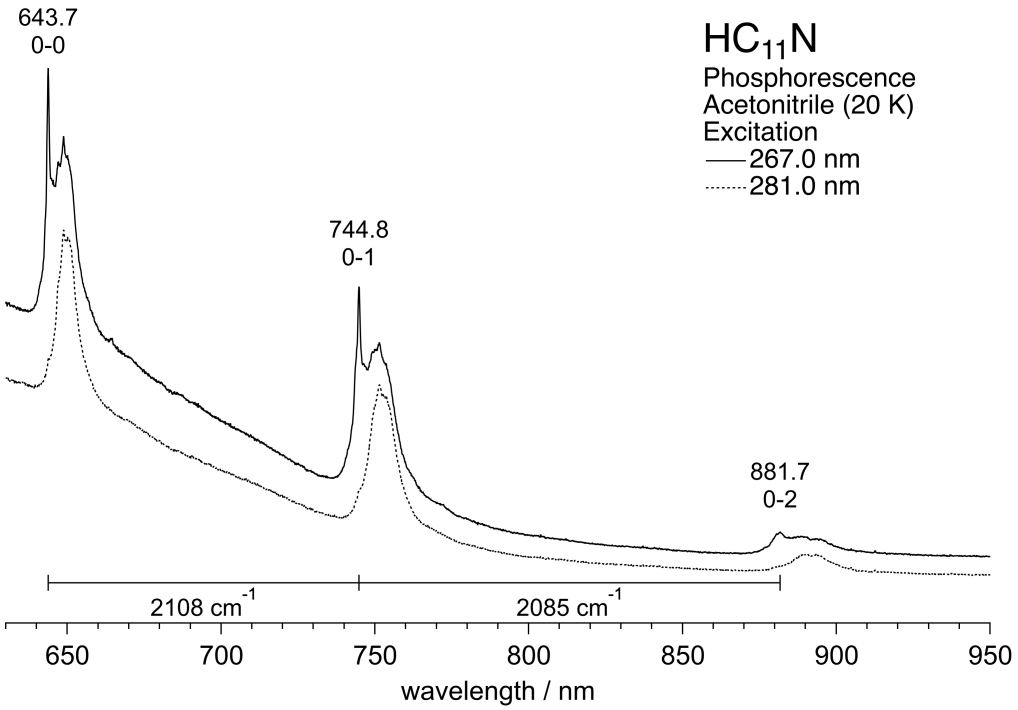

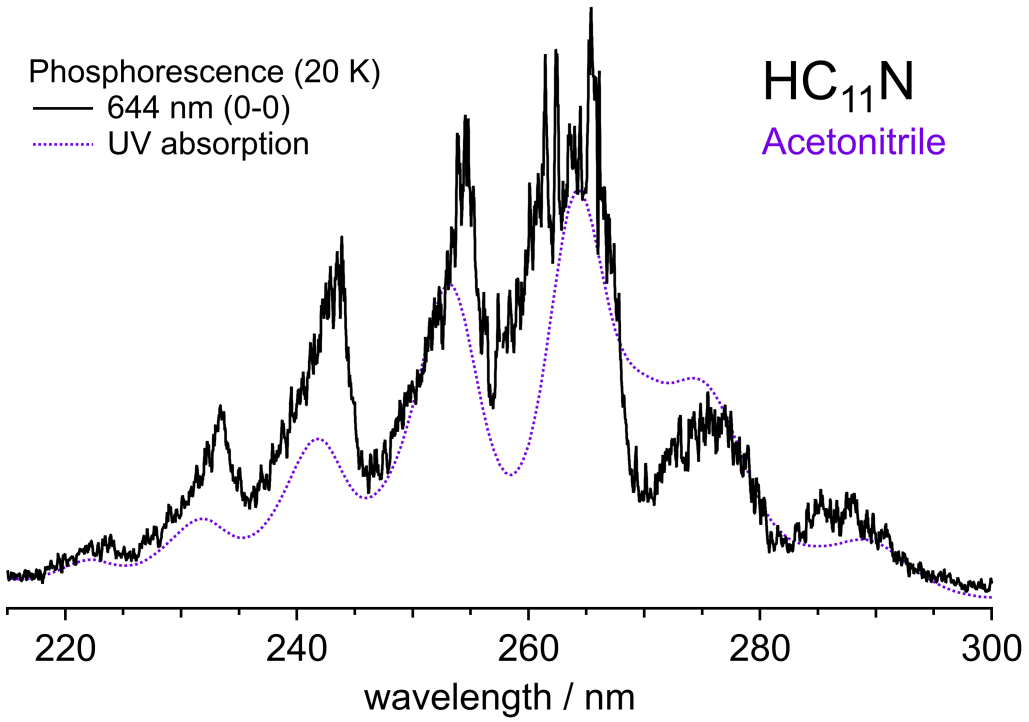

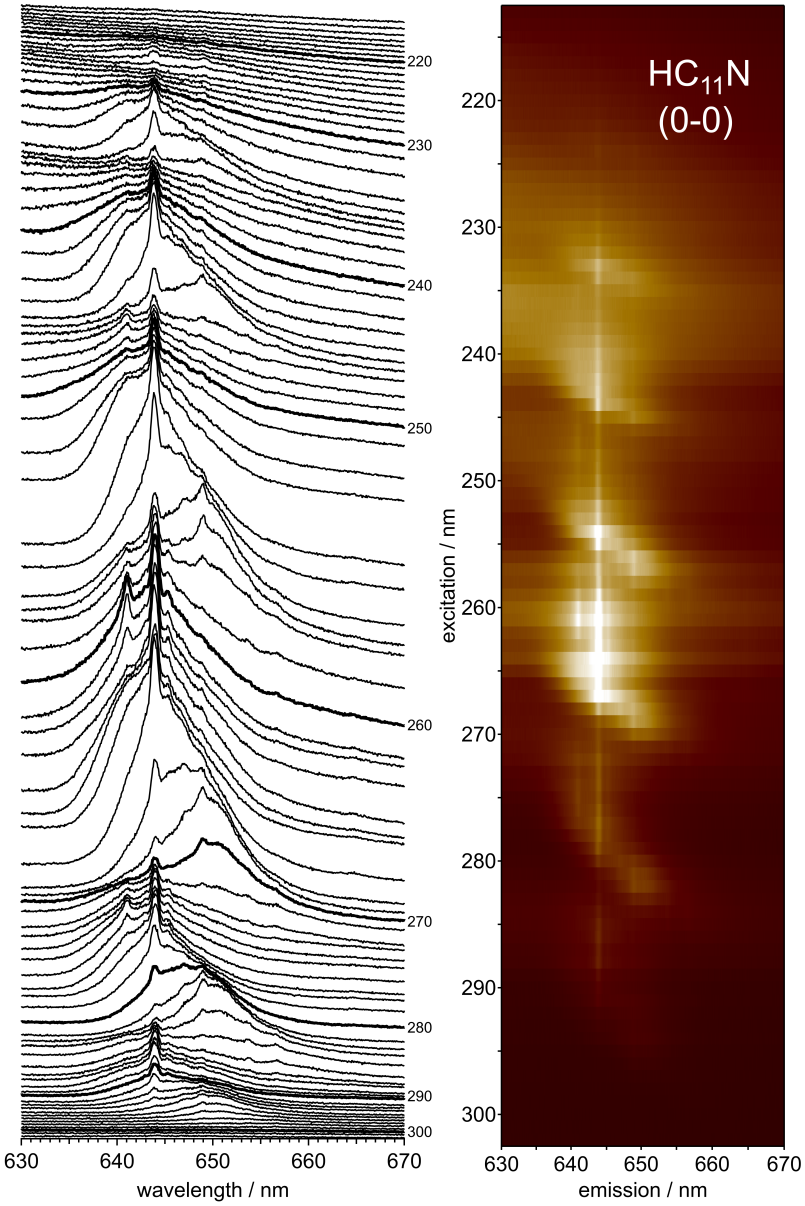
220
230
240
250
260
270
280
290
300
630
640
650
660
670
wavelength / nm
HC11N
(0-0)
excitation / nm
emission / nm

Highlights

- Phosphorescence of cyanopolyyne molecules of HC_9N and $HC_{11}N$ at 20 K
- Resonance Raman spectroscopy and IR spectra of HC_9N and $HC_{11}N$
- Solid acetonitrile or *n*-hexane matrix hosts provides multiple trapping sites

Declaration of interests

☒ The authors declare that they have no known competing financial interests or personal relationships that could have appeared to influence the work reported in this paper.

☐The authors declare the following financial interests/personal relationships which may be considered as potential competing interests: